Superalloys 2012: 12th International Symposium on Superalloys
Edited by: Eric S. Huron, Roger C. Reed, Mark C. Hardy, Michael J. Mills, Rick E. Montero, Pedro D. Portella, Jack Telesman
TMS (The Minerals, Metals & Materials Society), 2012

EFFECTS OF ALLOYING ELEMENTS ON ELASTIC, STACKING FAULT, AND DIFFUSION PROPERTIES OF FCC NI FROM FIRST-PRINCIPLES: IMPLICATIONS FOR TAILORING THE CREEP RATE OF NI-BASE SUPERALLOYS

C. L. Zacherl*[1], S. L. Shang[1], D. E. Kim[1,2], Y. Wang[1], and Z. K. Liu[1]
[1] Department of Materials Science and Engineering, The Pennsylvania State University, University Park, PA 16802, USA

Keywords: nickel alloys, elastic properties, stacking fault energy, diffusion coefficient, creep

Abstract

To understand the effects of alloying elements on the creep rate of Ni-base superalloys, factors entering into a secondary creep rate are calculated via first-principles calculations based on density functional theory for 26 $Ni_{31}X$ systems where X = Al, Co, Cr, Cu, Fe, Hf, Ir, Mn, Mo, Nb, Os, Pd, Pt, Re, Rh, Ru, Sc, Si, Ta, Tc, Ti, V, W, Y, Zr, and Zn. They are volume, elastic properties, stacking fault energy, and diffusivity. It is found that shear modulus, Young's modulus, and roughly stacking fault energy show inverse correlation to the atomic volume of the system. In addition, the closer the alloying elements to Ni, with respect to atomic volume and atomic number, the larger the predicted shear modulus, Young's modulus, and stacking fault energy. Diffusivity calculations show that mid-row 5d transition metal elements, particularly Re, Os, and Ir, have the highest activation barrier for diffusion, while far-right or far-left row placement elements such as Y, Zn, and Hf, have the lowest activation energy barriers for diffusion. A creep rate ratio of $\dot{\varepsilon}_{Ni_{31}X}/\dot{\varepsilon}_{Ni}$ is calculated and the effect of the alloying elements shows 13 systems have a decreased creep rate relative to Ni, while 13 systems have an increased creep rate relative to Ni.

Introduction

Materials scientist and engineers face two ever-present challenges with respect to Ni-base superalloys; increasing their service lifetime and increasing the upper limit of their operating temperatures. A major factor that inhibits materials scientist from meeting this challenge is creep deformation that occurs at high temperatures [1]. Creep is a time-dependent process and when it occurs, it is inelastic and irrecoverable. Without an intimate understanding of the effects of various elements on materials properties such as elastic constants, stacking fault energies, and diffusivities of alloying elements of Ni-base superalloys, it will be difficult to make the next generation of alloys with an increased creep resistance.

Another motivation for this work tied to creep deformation is the shrinking availability of rhenium in the Earth's crust, a material thought to have advantageous effects on the creep rate of Ni-base superalloys because of its low vacancy-solute exchange rates and high diffusion energy barriers [1-2]. In order to replicate the effects of Re on Ni-base superalloys, a fundamental understanding is needed on its effect to all aspects of a given creep model. Here, the secondary creep rate, featuring a back stress function and taking the stacking fault energy explicitly into account [3], can be expressed by [4-5]

$$\dot{\varepsilon} = AD\left(\frac{\gamma}{Gb}\right)^n\left(\frac{\sigma-\sigma_0}{E}\right)^m \quad (1)$$

where *A*, *m* and *n* are structure-dependent parameters with 4 given for *m* and 3 for *n* [5], *D* the diffusion coefficient, γ_{sf} the stacking fault energy, *G* the shear modulus, *b* the magnitude of Burgers vector, σ the flow stress, and *E* the Young's modulus. Diffusion properties [6-7], elastic constants [8], and stacking fault energies are all properties that can be calculated via first-principles calculations based on density functional theory at 0 K and all contribute to the creep process [4] in different ways. For example, elastic constants are important in understanding how the system will elastically deform, and can give other information on interatomic bonding [9] and mechanical stability [10]. Stacking fault energies depend on the ideal shear strength of the material [11-12] and are linked to materials phenomena related to the slip process [13]. Faster diffusion coefficients based on lower activation energy barriers to diffusion are directly linked to the speed of the creep rate, and it is still unclear which factors, such as solute size or electron configuration [1, 14], have the most impact on dilute impurity diffusion coefficients in fcc Ni.

In an effort to understand and minimize the creep rates of dilute fcc Ni binary alloys and gain a fundamental understanding of the effects of the various materials properties on the creep rate, the present work aims to predict the effects of 26 different alloying elements, X, on the 0 K elastic, stacking fault, and diffusion properties of fcc $Ni_{31}X$ systems through the use of first-principles calculations. Figure 1 shows the 26 alloys elements studied in the present work for the $Ni_{31}X$ systems:

															Al 13	Si 14	
Sc 21	Ti 22	V 23	Cr 24	Mn 25	Fe 26	Co 27	Ni 28	Cu 29	Zn 30								
Y 39	Zr 40	Nb 41	Mo 42	Tc 43	Ru 44	Rh 45	Pd 46										
	Hf 72	Ta 73	W 74	Re 75	Os 76	Ir 77	Pt 78										

Figure 1: 26 alloying elements and their atomic number studied in the present work in their approximate location on the periodic table.

The present work is unique in that it first isolates and discusses the effect of each alloying element, X, on the contributing factors, diffusion coefficient, stacking fault energy, and elastic constants, to Eq. 1 before discussing the effect of each contributing factor on creep rate.

[2] Now at: High performance materials R&D center, LG Hausys Ltd., Anyang, Gyeonggi, South Korea

Computational Procedure

First-principles calculations in the present work are performed using the VASP code [15] with the ion-electron interaction described by the projector augmented wave (PAW) method [16] and the exchange-correction functional depicted by the generalized gradient approximation (GGA) [17]. For the elastic constant VASP calculations, a 6×6×6 *k*-points mesh and a 350 eV energy cutoff of the wave function are used for the cubic 32-atom supercell. The stacking fault energy calculations are performed with a 10×8×3 (or 4×5×3) *k*-points mesh for 24-atom (or 72-atom) orthorhombic supercell and the 350 eV energy cutoff of the wave function. For the diffusion coefficient calculations, 8×8×8 *k*-points meshes are used for all cubic 32-atom configurations with a plane wave energy cutoff of 1.25 times the maximum energy cutoff for each respective $Ni_{31}X$ system. The energy convergence criterion of the electronic self-consistency is chosen to be at least 10^{-5} eV per atom for all the calculations. The reciprocal-space energy integration is performed by the Methfessel-Paxton technique [18] for structure relaxations. For the final calculations of total energies, electronic structures, and stresses, we adopt the tetrahedron method incorporating a Blöchl correction [19]. Due to the ferromagnetic nature of Ni, all the calculations are performed within the spin-polarized approximation.

Elastic constant calculation

First-principles elastic constants in the present work are determined by calculating the stresses in response to strains based on an fcc 2×2×2 supercell including 31 Ni atoms and one alloying element, X, with a 6×6×6 *k*-point mesh. The obtained stress-strain relationships are used to calculate the elastic constants via Hooke's law, pertaining to a temperature of 0 K and at a fixed volume, i.e., $c_{ij}(V)$. Here, strains of ±0.01 are used for Ni-base superalloys. Additional calculations using more strains (±0.007 and ±0.013) do not yield more accurate results for the elastic constants (error < 1%) and are unnecessary. More details about the calculations of first-principles elastic constants were given in our previous work [8], see also Refs. [9, 20-21].

Based on the obtained single crystal elastic constants c_{ij}'s, the polycrystalline aggregate properties such as bulk modulus (B), shear modulus (G), and Young's modulus can be estimated using the Voigt-Reuss-Hill approach [22]. The Voigt approach gives the upper bound of elastic properties in terms of the uniform strain, the Reuss approach gives the lower bound in terms of the uniform stress, and the Hill approach gives average between the Voigt and Reuss approaches. For crystals with cubic symmetry,

$$B_{Voigt} = (c_{11} + 2c_{12})/3 \quad \text{and} \quad B_{Reuss} = 1/(3s_{11} + 6s_{12}) \tag{2}$$

$$G_{Voigt} = (c_{11} - c_{12} + 3c_{44})/5 \quad \text{and} \quad G_{Reuss} = 5/(4ss_{11} - 4s_{12} + 3s_{44}) \tag{3}$$

where the matrix of elastic compliances s_{ij}'s can be calculated from the inverse of the matrix of elastic (stiffness) constants c_{ij}'s, and *vice versa*. From the B and G values based on the Voigt and Reuss approaches, a universal elastic anisotropy index A^U for crystal with any symmetry was proposed by Ranganathan *et al.*, [23]

$$A^U = {}^{5G_{Voigt}}\Big/_{G_{Reuss}} + {}^{B_{Voigt}}\Big/_{B_{Reuss}} - 6 \geq 0 \tag{4}$$

The departure of A^U from zero defines the extent of single-crystal elastic anisotropy, and $A^U = 0$ for locally isotropic single crystals. Note that for a crystal with cubic symmetry, the relationship between A^U and the commonly used Zener anisotropy ratio, A^Z, is $A^U = (6/5)\left(\sqrt{A^Z} - 1/\sqrt{A^Z}\right)^2$, where $A^Z = 2\,c_{44}/(c_{11} - c_{12})$ [9].

Stacking fault energy calculation

The generalized stacking fault energy is a measure of the energy penalty for shearing two adjacent planes, representing the nature of slip and involving both the stable (intrinsic) (γ_{SF}) and unstable (γ_{US}) stacking fault energies [11, 24-25]. For the {111} slip plane in fcc structure, the stable stacking fault configuration corresponds to a slip of $a_0/\sqrt{6}$ in the $<11\bar{2}>$ direction, resulting in the stacking …*ABC*|*BCABC*…, where a_0 is the fcc lattice parameter, *A*, *B*, and *C* are the different {111} layers.

In the present work, a simple alias shear deformation, i.e., only the top layer is displaced in the shearing direction and only atomic positions are allowed to relaxation, is employed to generate the stacking fault [12]. Here the shear deformation is performed on the close packed {111} plane along the $<11\bar{2}>$ directions of the $Ni_{23}X$ and $Ni_{71}X$ alloys, i.e. the (1×2×2) and (2×3×2) supercells, respectively, relative to a 6-atom orthorhombic cell with its lattice vectors **a**, **b**, and **c** parallel to $[11\bar{2}]$, $[\bar{1}10]$, and $[111]$, respectively, of the conventional fcc structure. More details about the calculations of stacking fault energy based on shear deformation were given in our previous work [26-27].

For the facility to usage and the prediction of creep rate for $Ni_{31}X$ alloys, the calculated stacking fault energies of $Ni_{23}X$ and $Ni_{71}X$ are fitted to,

$$\gamma(x) = \gamma_{Ni} + ax + bx^2 \tag{5}$$

where x is the mole fraction of alloying elements X and γ_{Ni} the stacking fault energy of fcc Ni.

Diffusion coefficient calculation

First-principles calculations are performed on a 32-atom 2×2×2 fcc Ni supercell including 31 Ni atoms and one alloying element, X. It is accepted that impurity elements diffuse in fcc crystals via the vacancy mechanism [28], so the present work demonstrates a method to calculate all factors entering into the equation for dilute impurity diffusion coefficient. The impurity diffusion coefficient is determined from the jump frequency of the impurity atom as it moves into a first neighbor vacant site via the unstable highest-energy saddle point. LeClaire and Lidiard represented the relationship between self-diffusion and impurity diffusion in the five frequency model [28] as

$$\frac{D_2}{D_0} = \frac{f_2}{f_0}\frac{w_4}{w_0}\frac{w_1}{w_3}\frac{w_2}{w_1} \tag{6}$$

where D_0 is the self-diffusion coefficient of the host lattice, fcc Ni in the present work, D_2 is the diffusion coefficient of the impurity atom, X, diffusion through Ni, f_2 is the correlation factor for impurity diffusion in the Ni-X system, and f_0 is the correlation factor for self-diffusion in fcc Ni. The remaining terms represent the five possible jumps occurring in the system.

To calculate the factors pertaining to the impurity diffusion coefficient, the following configurations are considered. $E(Ni_N)$ represents the energy of a perfect state (PS) of fcc supercell with N Ni atoms. $E(Ni_{N-1}X_1)$ represents the energy of a supercell with $N-1$ Ni atoms and an impurity, X, denoted by the abbreviation, (ps). $E(Ni_{N-1}V_1)$ represents the energy of a supercell with $N-1$ Ni atoms and a vacancy, V, at the initial state of the jump without an impurity present (IS). $E(Ni_{N-2}X_1V_1)$ represents the energy of the system with $N-2$ Ni atoms and both an impurity and vacancy present, and can represent the system when the impurity and vacancy are first nearest neighbors at the initial state of the impurity jump (is), second nearest neighbors (2NN), or when the impurity atom is in the saddle point, or transition state, (TS) between an initial and final vacancy configuration. In light of the five frequency model, one must take into account the difference in energy that it will take to form a vacancy when it is in the pure host matrix, ΔE_f^o surrounded by only host atoms, and when the vacancy forms adjacent to the impurity atom [29]. In the latter case, a solute-vacancy pair is formed, and its associated energy, known as the solute-vacancy binding energy, ΔE_b describes the energy it takes to bring an infinitely separated solute and vacancy into a solute-vacancy pair. The solute vacancy binding energy (where the negative sign keeps the convention consistent with the literature where a positive binding energy indicates favorable binding) is defined as [30]

$$-\Delta E_b = E(Ni_{N-2}X_1V_1) + E(Ni_N) - E(Ni_{N-1}X_1) - E(Ni_{N-1}V_1) \quad (7)$$

The diffusion coefficient can be written in Arrhenius form as [6]

$$D = D_0 exp(-Q/k_BT) \quad (8)$$

where D_0 is the diffusion prefactor based on the entropic contributions from the formation of vacancy and migration of the impurity atom, and Q is the activation energy for diffusion, based on the enthalpy of formation of the vacancy and migration of the impurity atom. In the present work, the temperature dependence of the correlation factor, f_2 and the activation energy for diffusion is calculated as [6, 31]

$$Q = \Delta E_f^o - \Delta E_b + \Delta E_m \quad (9)$$

where ΔE_m is the energy of vacancy migration defined as the difference between the transition state of the vacancy-solute exchange jump and the initial state of that jump, $\Delta E_m = E(Ni_{N-2}X_1V_1)_{TS} - E(Ni_{N-2}X_1V_1)_{IS}$. With Q defined, the remaining term to be defined in Eq. 8 is the diffusion prefactor, D_0. For the sake of simplicity and efficiency, D_0 can be estimated by treating the vibrational degrees of freedom near the saddle point as nearly simple harmonic oscillators [32]. This value was found to be on the order of 10^{-5} m^2/s for the dilute diffusion of transition metals in Ni [2, 31]. Thus, 10^{-5} m^2/s will be used for the diffusion prefactor in this work as an approximation, a value that well represents the experimental diffusion prefactor of pure Ni (8.5×10^{-5} – 17.7×10^{-5} m^2/s [33-35]).

In the present work, the saddle configuration (TS) is first predicted as the middle of the minimum energy path between the initial and final equilibrium vacancy configurations, and its energy is calculated using the nudged elastic band (NEB) method [17] within VASP. One image is used to calculate the TS. A 5.0 $eV/Å^2$ spring constant is used in all NEB calculations to nudge the image to the minimum energy path between the initial and final vacancy configurations.

Results and Discussion

Elastic constant calculation

Figure 2 illustrates the predicted shear moduli and Young's moduli of $Ni_{31}X$ alloys according to the Voigt approach as a function of equilibrium volume. It can be seen that the shear modulus decreases with increasing equilibrium volume, agreeing with the general trend observed for elastic properties relating moduli and equilibrium volume [9]. The shear modulus values of $Ni_{31}X$ alloys are affected greatly by the properties of the respective alloying element, such as, the larger shear moduli of $Ni_{31}Ru$ and $Ni_{31}Os$ are mainly caused by the larger shear moduli of pure elements Ru and Os compared to Ni [9]. Among all of the 26 alloying elements, the largest decrease of elastic properties of Ni is due to element Y, followed by Zr and Sc. Almost all X's (except for Co and Ru) decrease the shear modulus of Ni. Regarding Young's modulus, it shows almost the same behaviors as the shear modulus cases. For both shear and Young's moduli, it is generally observed that the 4d elements have the greatest impact on decreasing the moduli of the $Ni_{31}X$ systems with respect to that of pure Ni, and it also seems that the 3d elements have the smallest effect on the moduli of the system. In general, the closer the alloying elements to Ni, e.g. atomic volume and atomic number, the larger the predicted shear modulus and Young's modulus.

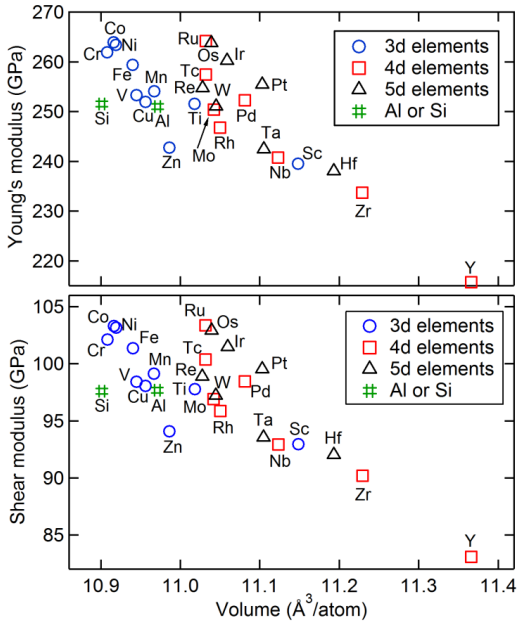

Figure 2: Calculated shear moduli and Young's moduli of $Ni_{31}X$ alloys at their equilibrium volumes based on the Voigt approach (see Eq. 2 and Eq. 3) at 0 K and without the zero point vibrational energies.

Stacking fault energy calculation

Based on Eq. 5, the obtained stacking fault energies for $Ni_{31}X$ alloys are plotted as a function of atomic number (Figure 3). It is found that all the alloying elements studied here decrease stacking fault energy of Ni, and similar to shear modulus and Young's modulus. As a result, the decrease of stacking fault energy of Ni is smaller by 3d transition metals alloying elements, compared to the 4d and 5d ones. The closer the equilibrium volume and atomic number of the alloys elements X to those of fcc Ni, the higher the stacking fault energy of $Ni_{31}X$ alloys. The same as for elastic properties, the largest decrease of stacking fault energy of Ni is caused by alloying element Y, followed by Zr, Mo, Nb, Re, W, etc.

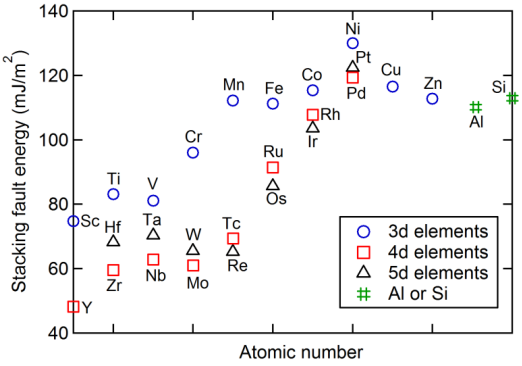

Figure 3: Calculated stacking fault energies of $Ni_{31}X$ alloys as a function of atomic numbers for 3d, 4d, and 5d alloying elements, as well as Al and Si, respectively.

Diffusion coefficient calculation

To understand the effect of each alloying element X, on the $Ni_{31}X$ systems, we turn to the activation energy for diffusion, Q, where a lower activation energy indicates faster diffusion of the impurity through the Ni matrix. Figure 4 plots activation energy calculated for some of the alloying elements by Janotti et al. [31] versus activation energies calculated in the present work, sorted by increasing atomic number for the 3d, 4d, and 5d transition elements. Other than the elements Y, Zn, Sc, Al, and Si, which were not previously calculated by Janotti et al. [31], excellent correlation with the present work for all elements with the exception of Zr, and to a lesser extent some of the 4d solutes. This can be attributed to the work of Janotti et al. [31] using the ultrasoft pseudopotential method [15], because the PAW [16] method used in the present work reconstructs the exact valence wave function with smaller core radii than the ultrasoft potentials, making the PAW a little more computationally expensive, but also more accurate. The previous studies on solute diffusion in Ni showed that there was no direct correlation between the activation energy barrier for diffusion and size of the impurity element [2, 31], results that are reproduced in the present work. The present work also shows that in general, 5d elements consistently have higher activation energies than the corresponding 4d element in the same row, while that trend does not hold for 3d elements. Additionally, Figure 4 shows that the elements with the highest activation energies calculated in the present work are all 5d solutes, Re, Os, and Ir, exist in the middle of their transition row, not the far right or left. The four elements with the lowest activation energies of the $Ni_{31}X$ systems, Y, Zn, Hf, and Sc, are also the four elements with the lowest shear moduli presented in Figure 2.

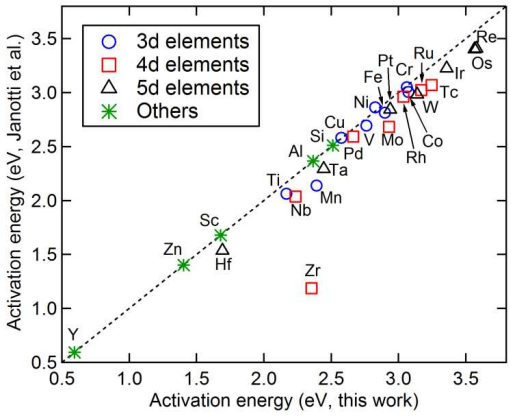

Figure 4: Diffusion activation energy for the 26 $Ni_{31}X$ systems and the activation energy for self-diffusion in Ni plotted from the present work versus diffusion activation energies from Janotti, et al. [31]. Note, Y, Zn, Sc, Al, and Si were not studied in the previous work.

Creep rate predictions

The preceding results sections show how each factor entering into the creep rate in Eq. 1, elastic constants, stacking fault energy, and diffusivity is affected by the impurity element, X, in the 26 $Ni_{31}X$ systems. The next step is to combine all of the results to gain a more holistic understanding of the effect of each alloying element on the creep rate of single crystal $Ni_{31}X$ systems compared to pure Ni. To do this, the relative creep rate is taken as a ratio of $ln(\dot{\varepsilon}_{Ni_{31}X}/\dot{\varepsilon}_{Ni})$ to demonstrate which elements reduce the creep rate and which elements increase the creep rate with respect to pure Ni. The effect of using a ratio means that the structural parameter, A, (in Eq. 1), diffusion prefactor, D_0, (in Eq. 8), and the flow stress, σ, (in Eq. 1), cancel out. The Burgers vector for each $Ni_{31}X$ system is calculated based on the equilibrium volume presented in Figure 2. Figure 5 (a) plots the relative creep rate for each $Ni_{31}X$ system based on increasing atomic number for each transition element row. An immediate observation shows that in general, 5d elements lower the creep rate compared to pure Ni more than 4d elements, and 4d elements lower the relative creep rate more than 3d elements. Figure 5 (b) shows the relative creep rate ratio in the periodic table, where a negative (green) creep rate indicates a slower creep rate with the addition of element X, and a positive (red) creep rate ratio indicates that the addition of elements X increases the creep rate in the system.

Of the 26 $Ni_{31}X$ systems, 13 have slower creep rates than Ni (X = Re, Os, Ir, Tc, W, Ru, Cr, Co, Mo, Rh, Pt, Fe, V), and 13 have faster creep rates than Ni (X = Pd, Cu, Ta, Si, Zr, Mn, Al, Nb, Ti, Hf, Sc, Zn, and Y). The three $Ni_{31}X$ systems with the slowest creep rates are 5d elements, Re, Os, and Ir.

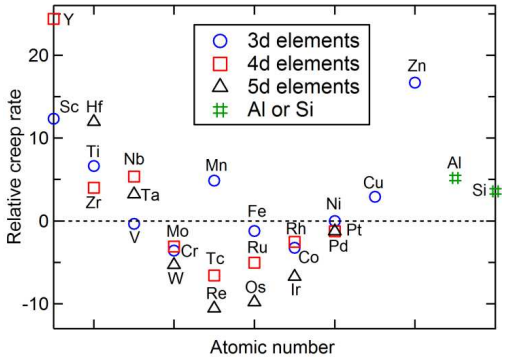

(a)

										Al 5.215	**Si** 3.585
Sc 12.34	**Ti** 6.647	**V** -0.369	**Cr** -3.590	**Mn** 4.871	**Fe** -1.203	**Co** -3.244	**Ni** 0	**Cu** 2.904	**Zn** 16.69		
Y 24.39	**Zr** 4.022	**Nb** 5.348	**Mo** -3.072	**Tc** -6.594	**Ru** -5.042	**Rh** -2.513	**Pd** 1.951				
	Hf 11.97	**Ta** 3.219	**W** -5.303	**Re** -10.55	**Os** -9.810	**Ir** -6.745	**Pt** -1.267				

(b)

Figure 5: Relative creep rate ratio plotted in (a) as a function of increasing atomic number across transition element rows and (b) in the periodic placement showing rates slower than pure Ni (green) and rates higher than pure Ni (red).

However, of the three $Ni_{31}X$ systems with the faster creep rate, two are from the 3d rows, Sc, and Zn, and one is from the 4d row, Y. More interesting to note is that Re, Os, and Ir exist in the middle of the 5d row, while Sc, Zn, and Y are on the far right or far left placement of their respective d-shell electron rows. This indicates that perhaps the creep rate has more to do with electronic configuration rather than atomic size, lattice strain, or other factors. This conclusion is further supported by Figure 5 where it is observed that aside from Mn, the $Ni_{31}X$ systems with significantly reduced creep rates from Ni are all clustered in the same four columns of the transition metal rows. Another interesting observation lies in the fact that Sc, Hf, Zr, and Y all seem to have the same effects on the $Ni_{31}X$ systems, regardless of the property of interest. They decrease the shear modulus of the system, decrease the Young's modulus of the system, have the lowest stacking fault energy of all of the systems, and have four of the five lowest activation energies for diffusion of all of the systems. On the other hand, Re and Os consistently have the opposite effects on the $Ni_{31}X$ systems, increasing the moduli, increasing the stacking fault energy, and having high activation barriers for diffusion. Further study of the electronic structures of these systems, particularly between Nb and Mo, and Ta and W, where only one electron can cause and increase or decrease in the creep rate, is desirable and would greatly aid in the understanding of the factors contributing to creep rate in Ni-base superalloys.

Conclusions

First-principles calculations based on density functional theory are used in the present work to predict 0 K elastic properties, stacking fault energies, and diffusion coefficients of 26 $Ni_{31}X$ systems, where X = Al, Co, Cr, Cu, Fe, Hf, Ir, Mn, Mo, Nb, Os, Pd, Pt, Re, Rh, Ru, Sc, Si, Ta, Tc, Ti, V, W, Y, Zr, and Zn. Elastic properties, including shear modulus and Young's modulus, and most stacking fault energies of the 26 $Ni_{31}X$ systems show an inverse correlation to the atomic volume of the system. It is shown that mid-row transition elements, such as 5d Re, Os, and Ir, and 4d Tc and Ru increase the activation barrier for diffusion in the $Ni_{31}X$ systems, while in comparison, elements at the end of the rows such as Y, Zn, and Hf significantly decrease the activation barrier for diffusion when compared to pure Ni. Finally, a relative creep rate is calculated for each $Ni_{31}X$ system and it is shown that Re, Os, Ir, Tc, and W have the most significant effect to decrease the creep rate compared to pure Ni. In general, it is also observed that 5d elements have a more significant effect on enhancing creep properties of the $Ni_{31}X$ systems than the 4d elements, and 4d elements a more significant effect than 3d elements.

Acknowledgements

This work was funded by the Office of Naval Research (ONR) under contract No. N0014-07-1-0638 and the Center for Computational Materials Design (CCMD), a National Science Foundation (NSF) Industry/University Cooperative Research Center at Penn State (IIP-1034965) and Georgia Tech (IIP-1034968). First-principles calculations were carried out in part on the LION clusters at the Pennsylvania State University supported by the Materials Simulation Center and the Research Computing and Cyberinfrastructure unit at The Pennsylvania State University, and in part by the high performance computing resources at ERDC as part of the Department of Defense High Performance Computing Modernization Program. We thank ONR program manager David Shifler for his support and encouragement. The authors would like to thank J. X. Zhang and A. D. Patel from Carpenter Technology Corporation and Paul Mason from ThermoCalc AB for mentoring the CCMD projects.

References

[1] RC Reed, The superalloys: fundamentals and applications, Cambridge, UK: Cambridge University Press; 2006.

[2] M Krčmar, CL Fu, A Janotti, RC Reed, Diffusion rates of 3d transition metal solutes in nickel by first-principles calculations, Acta Materialia, 2005; 53: 2369-76.

[3] C Barrett, O Sherby, Influence of stacking-fault energy on high-temperature creep of pure metals, Trans Met Soc AIME, 1965; 223: 1116.

[4] Z Guo, AP Miodownik, N Saunders, JP Schille, Influence of stacking-fault energy on high temperature creep of alpha titanium alloys, Scripta Materialia, 2006; 54: 2175-8.

[5] ZL Guo, N Saunders, AP Miodownik, JP Schillé, Quantification of high temperature strength of nickel-based superalloys, Materials Science Forum, 2007; 546-549: 1319-26.

[6] M Mantina, Y Wang, LQ Chen, ZK Liu, C Wolverton, First principles impurity diffusion coefficients, Acta Materialia, 2009; 57: 4102-8.

[7] JR Manning, Correlation Factors for Impurity Diffusion. bcc, Diamond, and fcc Structures, Physical Review, 1964; 136: A1758-A66.

[8] D Kim, SL Shang, ZK Liu, Effects of alloying elements on elastic properties of Ni by first-principles calculations, Computational Materials Science, 2009; 47: 254-60.

[9] SL Shang, A Saengdeejing, ZG Mei, DE Kim, H Zhang, S Ganeshan, Y Wang, ZK Liu, First-principles calculations of pure elements: Equations of state and elastic stiffness constants, Comput Mater Sci, 2010; 48: 813-26.

[10] JF Nye, Physical Properties of Crystals: Their Representation by Tensors and Matrices, New York: Oxford University Press; 1985.

[11] S Ogata, J Li, S Yip, Ideal pure shear strength of aluminum and copper, Science, 2002; 298: 807-11.

[12] M Jahnatek, J Hafner, M Krajci, Shear deformation, ideal strength, and stacking fault formation of fcc metals: A density-functional study of Al and Cu, Phys Rev B, 2009; 79: 224103.

[13] MF de Campos, Selected values for the stacking fault energy of face centered cubic metals, Mater Sci Forum, 2008; 591-593: 708-11.

[14] RC Reed, T Tao, N Warnken, Alloys-By-Design: Application to nickel-based single crystal superalloys, Acta Materialia, 2009; 57: 5898-913.

[15] G Kresse, J Furthmuller, Efficient iterative schemes for ab initio total-energy calculations using a plane-wave basis set, Physical Review B, 1996; 54: 11169-86.

[16] G Kresse, D Joubert, From ultrasoft pseudopotentials to the projector augmented-wave method, Physical Review B, 1999; 59: 1758-75.

[17] JP Perdew, Y Wang, ACCURATE AND SIMPLE ANALYTIC REPRESENTATION OF THE ELECTRON-GAS CORRELATION-ENERGY, Phys Rev B, 1992; 45: 13244-9.

[18] M Methfessel, AT Paxton, HIGH-PRECISION SAMPLING FOR BRILLOUIN-ZONE INTEGRATION IN METALS, Phys Rev B, 1989; 40: 3616-21.

[19] PE Blöchl, Projector Augmented-Wave Method, Phys Rev B, 1994; 50: 17953-79.

[20] SL Shang, Y Wang, ZK Liu, First-principles elastic constants of alpha- and theta-Al2O3, Appl Phys Lett, 2007; 90: 101909.

[21] SL Shang, G Sheng, Y Wang, LQ Chen, ZK Liu, Elastic properties of cubic and rhombohedral BiFeO3 from first-principles calculations, Phys Rev B, 2009; 80: 052102.

[22] G Simmons, H Wang, Single Crystal Elastic Constants and Calculated Aggregate Properties, Cambridge (Mass.): MIT press; 1971.

[23] SI Ranganathan, M Ostoja-Starzewski, Universal elastic anisotropy index, Phys Rev Lett, 2008; 101: 055504.

[24] S Ogata, J Li, Y Shibutani, S Yip, Ab initio Study of Ideal Shear Strength, Solid Mech Appl, 2004; 115: 401-10.

[25] H Van Swygenhoven, PM Derlet, AG Froseth, Stacking fault energies and slip in nanocrystalline metals, Nat Mater, 2004; 3: 399-403.

[26] SL Shang, WY Wang, Y Wang, Y Du, JX Zhang, AD Patel, ZK Liu, Temperature-dependent ideal strength and stacking fault energy of fcc Ni: A first-principles study of shear deformation In: Under Review, Journal of Physics and Condensed Matter; 2012.

[27] SL Shang, CL Zacherl, Y Wang, Y Du, ZK Liu, Effects of alloying elements and temperature on the elastic properties of

dilute Ni-base superalloys from first-principles calculations, to be submitted, 2012.

[28] AD Leclaire, AB Lidiard, CORRELATION EFFECTS IN DIFFUSION IN CRYSTALS, Philosophical Magazine, 1956; 1: 518-27.

[29] H Mehrer, Diffusion in Solids, Berlin: Springer; 2007.

[30] C Wolverton, Solute–vacancy binding in aluminum, Acta Materialia, 2007; 55: 5867-72.

[31] A Janotti, M Krčmar, CL Fu, RC Reed, Solute Diffusion in Metals: Larger Atoms Can Move Faster, Physical Review Letters, 2004; 92: 085901.

[32] GH Vineyard, Frequency factors and isotope effects in solid state rate processes, Journal of Physics and Chemistry of Solids, 1957; 3: 121-7.

[33] H Bakker, A Curvature in the In D versus 1/T Plot for Self-Diffusion in Nickel at Temperatures from 980 to 1400°C, physica status solidi (b), 1968; 28: 569-76.

[34] K Maier, H Mehrer, E Lessmann, W Schüle, Self-diffusion in nickel at low temperatures, physica status solidi (b), 1976; 78: 689-98.

[35] AB Vladimirov, VN Kaigorodov, SM Klotsman, IS Tracktenber, DIMETA 82, Proceedings of International conference on diffusion in metals and alloys, In: FJ Kedves, DL Beke editors: Trans. Tech. Publications; 1982.